X-692-70-270
PREPRINT

NASA TM X- 63996

ENERGY TRANSFER AT COLLIDING STREAMS IN THE SOLAR WIND

L. F. BURLAGA
K. W. OGILVIE
D. H. FAIRFIELD
M. D. MONTGOMERY
S. J. BAME

JULY 1970

GSFC
GODDARD SPACE FLIGHT CENTER
GREENBELT, MARYLAND

X-692-70-270

ENERGY TRANSFER AT COLLIDING STREAMS IN THE SOLAR WIND

by

L. F. Burlaga
K. W. Ogilvie
D. H. Fairfield

Laboratory for Extraterrestrial Physics
Space Plasma Physics Branch
NASA Goddard Space Flight Center
Greenbelt, Maryland

and

M. D. Montgomery
S. J. Bame

Los Alamos Scientific Laboratory
Los Alamos, New Mexico

July 1970

Abstract

Processes occurring when a fast stream of solar plasma overtakes a slower one are investigated using Explorer 34 and Vela 4B measurements of the relevant proton, α-particle, electron and magnetic field parameters for 3 events. The protons are heated by an amount such that the maximum thermal speed approximately equals the relative speed of the 2 streams. The proton thermal anisotropy does not increase, indicating that either the heating is not due to hydromagnetic wave damping alone, or both MHD heating and an isotropization mechanism are operative. The α-particles are heated in proportion to the protons, but the electron temperature does not measurably increase. The magnetic field intensity reaches a maximum after the density, and the field fluctuations with frequencies $(1.5 \times 6) \times 10^{-3}$ Hz are unusually high in the hot spots but not adjacent to them. The hypothesis that such fluctuations are propagating from colliding streams is not supported. The proton density and temperature profiles are consistent with the results of a non-steady, non-linear adiabatic fluid model. A hydromagnetic 3-fluid model with heat conduction is needed to explain the other observations.

I. Introduction

Jets and streams are commonly found in large scale flows in astrophysics. In particular, it is known that motions in the solar wind are not uniform and that several parameters are correlated with gradients in the bulk speed. Abnormally high ion temperatures at the leading edge of high speed streams were noted qualitatively by Neugebauer and Snyder (1966a). Burlaga and Ogilvie (1970) demonstrated this quantitatively, and argued that the Kelvin-Helmoltz instability was not the cause of the heating. Exceptionally high densities and magnetic field intensities are usually observed ahead of the temperature increases when the speed begins to increase (Neugebauer and Snyder (1967), Lazarus et al. (1967)). Davis et al. (1966) and Neugebauer and Snyder (1966b) showed that the variance of the magnetic field tends to be unusually high at the leading edge of high speed streams.

The purpose of this research is to study the dominant physical processes that occur at large positive bulk speed gradients in the solar wind. In contrast to the earlier work, which emphasized correlations between 2 or 3 variables for extended periods of time, our approach is to use many types of measurements for just 3 events.

Section III presents observations of bulk speed, density, magnetic field intensity, magnetic field fluctuations, proton temperature (T) and anisotropy, electron temperature (T_e) and helium temperature for 3 events. Section IV shows that the heating may be the result of adiabatic compression.

II. Instrumentation and Orbits

The Explorer 34 plasma experiment has been described in detail elsewhere by Ogilvie, McIlwraith and Wilkerson (1968). The spectra of hydrogen and helium ions are observed separately, so the helium spectrum is completely uncontaminated by protons. The proton spectrum, however, may be slightly contaminated by helium when the helium density is high. Each spectrum is made up of 16 observations, and takes 15 spins to record, each of duration 2.56 sec. The angular acceptance of the instrument is $\pm 9^{\circ}$ in a plane containing the spin axis, which is oriented perpendicular to the plane of the ecliptic. The acceptance is 2.5° in the azimuthal direction, but counting is integrated over 360°, so that the velocity distributions projected onto the ecliptic are completely covered.

The Explorer 34 magnetic field experiment (see Fairfield 1969) consists of a triaxial fluxgate magnetometer with ± 32 gamma range and $\pm .16$ gamma digitization error in the interplanetary region. The experiment produces a vector field sample every 2.56 seconds; 8 point (20.5 second) averages are used in this paper.

The Vela 4B plasma experiment has been described elsewhere (Montgomery et al. 1968, and Montgomery et al. 1970) so only a brief description is given here. The instrument is a hemispherical plate electrostatic analyzer having a 110° polar acceptance angle centered on the spacecraft equatorial plane and an azimuthal resolution of 2.6°. The data required to generate a set of fluid parameters describing the electron component of the plasma are collected during one revolution of the spacecraft requiring

64 sec. These data consist of 16 differential energy spectra each made up of 20 contiguous energy channels between 14 and 1600ev with 28% spacing. 0.375 sec. is required to acquire each energy spectrum, and adjacent spectra are 4 sec. (22.5° in azimuth) apart. A set of high resolution positive ion data is collected during a 6 sec. interval every other revolution of the spacecraft as the acceptance fan of the instrument sweeps past the sunward direction. These data consist of 7 differential energy-per-charge (E/Q) spectra each consisting of 24 contiguous energy channels between 0.32 to 5.5 keV/Q with ~12% spacing. The measurement of each spectrum requires ~0.190 sec. and the spectra are taken 5.6° apart in azimuth.

The electron fluid parameters are calculated by evaluating the appropriate moments of the measured electron velocity distribution, while the proton parameters are given by a least squares fit to a bi-Maxwellian velocity distribution (see Montgomery et al., 1968, 1970). Transverse and longitudinal alpha particle temperatures are derived as follows:

a. Longitudinal. The three E/Q spectra containing the largest number of counts due to alpha particles are summed, and the resulting velocity distribution is fit by least squares to a Maxwellian distribution. The alpha particle bulk speed is assumed equal to the previously determined proton bulk speed (Ogilvie et al. 1968) and Robbins et al. (1970), and, in order to minimize proton contamination, only the part of the alpha velocity distribution that extends above the assumed bulk speed is used.

b. Transverse. The three E/Q channels at each angle centered on the value of E/Q corresponding to the alpha bulk speed are summed. A Maxwellian fit to the resulting angular distribution gives the

transverse alpha temperature.

Orbits

The Explorer 34 orbit about the earth was highly elliptical with apogee $34R_E$, inclination 67^o and period 4.3 days (see Behannon et al. 1968). The Vela 4B orbit is nearly circular with radius $19R_E$, inclination 58^o, and period 4.7 days. During the intervals discussed below, the distance between Explorer 34 and Vela 4B ranged between $17R_E$ and $52R_E$.

III. Observations

From the Explorer 34 plasma data presented by Burlaga and Ogilvie (1970) we selected three regions with increasing bulk speed and anomalously high temperature: 1200 UT on day 180 (June 29, 1967) to 2000 UT on day 181 (June 30), 1200 UT on day 198 (July 17) to 0400 UT on 199 (July 18), and 0100 UT on 315 (November 11) to 1200 UT on 316 (November 12). These intervals were selected because, 1) the velocity gradient was large and accompanied by a clear peak in proton temperature, 2) the velocity gradient occurred when Explorer 34 was near apogee with good interplanetary coverage for a day before and a day after the gradient, 3) Vela 4B measurements were available and 4) no shock occurred in the intervals.

The observations to be discussed are shown in Figure 1, 2, and 3; the continuous lines are from Explorer 34 data, and the heavy bars, dots, shaded bars and broken lines are Vela 4B results. These figures show the effects noted by earlier workers and attributed to colliding streams, namely: 1) an increase in density, n, just before the positive bulk speed gradient, 2) an increase in magnetic field intensity, B, to a value exceeding 10 gamma near the gradient, and 3) an abnormally high temperature at the bulk speed gradient. The large temperature increase is shown quantitatively by the plot of $\Delta T = T - (.036V - 5.56)^2$ which is the difference between the observed proton temperature and that calculated from the bulk speed using the (V,T) relation of Burlaga and Ogilvie (1970). Table I shows that the mean thermal speed, V_T, corresponding to the maximum temperature is equal, within the experimental errors, to the difference between the 3-hr averages of the bulk speed on either side of the hot spot defined by $\Delta T \geq 5 \times 10^4 {}^{o}K$.

New features of these data are

1) The electron temperature, T_e, (Figures 1 and 2) does not increase significantly in the region where protons are heated. No electron data exists for Figure 3;

2) The proton temperature anisotropy, Figures 1, 2 and 3, measured by T_{max}/T_{min} (See Hundhausen et al., 1967) is not enhanced in the heating region;

3) The energy density, $E=B^2/(8\pi) + nk(T_e+T)$ increases in the gradient region, at first because of the density increase, and at later times primarily because of the high B; and

4) The maximum magnetic field intensity may occur before the proton temperature peak (Figures 2 and 3) or after it (Figure 1).

We have assumed that the plasma was homogeneous on a scale of the Vela 4B-Explorer 34 separation. That this is so is indicated by the very good agreement between the speeds and proton temperatures measured at the 2 spacecraft. The Vela 4B densities were 2 times the Explorer 34 densities, but when the Vela 4B measurements are normalized with respect to Explorer 34 measurements one finds that they show virtually the same behavior (Figures 1, 2, 3), indicating that the constant difference is probably instrumental. The reason for this difference is not yet understood, and it is not known which is correct.

Note that the density steadily decreases in the region where the bulk speed increases in Figures 1, 2 and 3. This is a very general result which can be seen at positive speed gradients in published data (Neugebauer and Synder (1967), Lazarus et al.(1967)) and is also common in Explorer 34 data.

Note that the magnetic field intensity does not increase simultaneously with the density ahead of the bulk speed gradient, but rather increases to a maximum after the density begins to fall. Thus, the pressure tends to be constant across the hot spot even though it is relatively high throughout the interaction region. This effect is not peculiar to these 3 events - it can be seen at other gradients in Explorer 34 data as well as at some of the gradients in other published data (Neugebauer and Snyder, 1966a, Figure 1; Neugebauer and Snyder 1966b, Figures 1 and 3). Figures 1,2 and 3 suggest that the heating, measured by ΔT, is related to the magnitude of the bulk speed gradient. This is shown more clearly in Figure 4, where $\Delta T(t)$ and $\Delta V/V = (V(t+3\ hr) - V(t-3\ hr))/ V(t)$ (computed from 3-hr averages of V) are plotted as a function of time for each of the 3 events. The former quantity represents the temperature excess over that predicted using the V-T relation, and the latter the fractional bulk speed change over the six hour interval.

Magnetic Field Fluctuations. Magnetic field fluctuations in the hot spots were studied by computing power spectra for consecutive 3 hour intervals using 20.5 second average field vectors. Figure 5 illustrates representative spectra for regions within and outside of the heating region. P_F represents power in the field magnitude and reflects fluctuations in a compressional magnetoacoustic wave mode while P_Y represents power in a component perpendicular to the average field direction and is dominated by transverse waves. Enhanced power is present in the heating region, and the transverse fluctuations predominate over the longitudinal fluctuations as is normally true in the interplanetary medium. These spectra cannot be well described by an inverse frequency dependence but they are generally bounded by the f^{-1} and f^{-2} dashed lines shown in the figure.

Variations of the fluctuations throughout the intervals of Figures 1-3 were studied by integrating power in the frequency region 1.5×10^{-3}Hz - 6×10^{-3}Hz. Lower frequencies were omitted to remove wavelengths whose scale was comparable to the interaction region. The higher frequencies were removed because of an instrumental peak near 7×10^{-3} Hz (gaps in the data of Figure 5) and the possible effects of waves associated with the presence of the earth (Fairfield 1969). Figure 6 illustrates this integral power in the transverse modes $P_{XY}\equiv(P_X^2 + P_Y^2)^{\frac{1}{2}}$ and the longitudinal mode P_F along with the velocity and the excess temperature. Enhanced field fluctuations occur in the hot spots in all three events. Note, however, that the power levels drop to very low values (Sari and Ness, 1969) just outside the hot spots.

Explorer 34 Proton Spectra. To determine whether changes in the shape of the proton spectra occur as a result of heating, we compare the 30-min average spectra in the hot spots with corresponding spectra outside the hot spots as follows. Using the observed counts $C_{obs}(V_i)$, the spectra are first fitted empirically as described by Burlaga and Ogilvie (1968), without assuming a Maxwellian, and fluid parameters n, V, T are obtained. Then the counts $C_{calc}(V_i)$ which would be observed in the various energy channels are computed for these parameters on the assumption of a Maxwellian distribution. If the observed distribution were Maxwellian, a plot of C_{calc} versus C_{obs} would show points scattered about the line $C_{calc}=C_{obs}$. If there were a high random energy tail, the computed temperature would be too high and the counts C_{calc} would be greater than C_{obs} for $|V_i-V| > V_{th}$ where V_{th} is the proton thermal velocity.

The right panel of Figure 7 shows C_{calc} vs C_{obs} for the heating regions in Figures 1, 2 and 3; the corresponding plot for the other regions is shown in the left panel of Figure 7. All three regions are shown in the same plot to improve the statistics and because no significant differences between the 3 events could be seen. The open circles refer to points corresponding to $V_i>V$ and the dots to $V_i<V$. Figure 7 shows the following:

1). to zeroth approximation both the heating and non-heating regions have Maxwellian spectra.

2). to 1st approximation the spectra in the heating and non-heating regions are the same and show a deviation from Maxwellian which is characteristic of a high energy tail.

He^{++} Measurements. Jokipii and Davis (1969) have pointed out that the damping of hydromagnetic waves in a plasma (Barnes, 1966) tends to produce the same velocity distribution in the component ions, for example helium and hydrogen in the interplanetary medium, leading to $T_\alpha/T_p = 4$. Solar wind measurements (Neugebauer and Snyder, 1966a; Hundhausen et al., 1967; Robbins et al., 1970; Ogilvie and Wilkerson, 1969), show the ratio T_α/T_p typically to have the value ~3.5. Barnes (1970) noted that helium is heated more strongly than protons by waves when $\frac{T_\alpha}{T_p} \gtrsim 4$. Processes near colliding streams might tend to produce thermal equilibrium, leading to lower values to T_α/T_p tending to unity. We therefore examine the measured values of T_α/T_p, with the primary aim of distinguishing between one and 3.5.

Vela 4B measurements of the transverse and longitudinal alpha temperatures are plotted versus time in Figure 8 for the event on days 180 and 181. The figure shows that the α temperature profile is the same as that of the mean proton temperature and that the ratio of the α and proton temperature is nearly constant at a value which is close to 4 and decidedly greater than 1.

The Explorer 34 alpha observations presented some difficulties because of the low net counting rate caused by an electronic background (Ogilvie and Wilkerson, 1969). To improve the accuracy, T_α spectra were averaged for successive 30 minute intervals. This may give an artifically large temperature if the bulk speed varies during the 30 minute intervals, but such periods were identified by examining the variance of the bulk speed, computed from individual proton

spectra at 3 minute intervals. To compute T_α/T_p, the proton temperatures from 30 minute average spectra were used, except when these differed by >50% from individual temperature measurements, when the corresponding hour averages were employed. When the proton bulk speed differed from the α bulk speed by >15 km/sec, no ratio was computed.

Using the above procedure,4 average spectra were obtained in the heating region in Figure 3 for which α and proton temperature could be calculated, leading to the value $T_\alpha/T_p \sim 2.8\pm.7$. Comparing this with the corresponding ratio $T_\alpha/T_p=3.2\pm1.3$ for 2 average spectra outside the heating region in Figure 3, one finds that the α particles were heated in the same proportion as the protons. Unfortunately no α particle temperatures could be obtained for the heating regions in Figures 1 and 2 from the Explorer 34 data. Measurements of α temperatures are available for other hot spots discussed by Burlaga and Ogilvie (1970) and the corresponding ratio T_α/T are shown in Table II. In every case, the T_α/T ratio is more consistent with 4 than with 1, indicating that the α particles and protons are heated at hot spots almost proportionally. In fact the average ratio for the heating regions $T_\alpha/T=3.5$ is essentially the same as the mean value $T_\alpha/T=3.7$ reported by Robbins et al. (1970) for the period July 1965 to July 1967.

TABLE I

Relation between ΔV and V_T

Event in Figure	ΔV(km/sec)	V_T(km/sec)
1	88	81
2	89	76
3	99	98

TABLE II

Ratio of α to proton temperatures at hot spots

		T_α/T	#30 min av. spectra
210	0000-0400	$4.0\pm.5$	4
223	1000-1600	$3.3\pm.4$	3
245	0230-0300	5.8	1
256	0930-1000	3.6	1
271	0700-2300	4.0 ± 1.7	6
315	2000-316, 0200	$2.8\pm.7$	4
	Average	3.9	

IV Summary and Discussion

The above collection of experimental observations gives the following results describing the interaction of a high speed solar plasma stream with slower moving solar wind:

1) The proton temperature is anomalously high at the velocity gradient, the excess being on the order of 10^5°K.
2) The peak in proton temperature occurs where the change in bulk speed is greatest.
3) The density peaks ahead of the temperature, when the speed just begins to increase.
4) The maximum density is ~ 3 times the ambient value.
5) There is no significant zeroth or first order difference between the velocity distributions inside and outside the heating region; they are Maxwellian to zeroth order.
6) There is no significant difference between proton anisotropies inside and outside the heating region.
7) Proton and α temperatures increase in the same proportion in the hot spots.
8) There is no significant increase in the electron temperature at the velocity gradient.
9) The magnetic field intensity peaks after the density in the region of the velocity gradient, and the peak is not coincident with the temperature peak.
10) Magnetic fluctuations in the range 1.5×10^{-3} Hz- 6×10^{-3} Hz are enhanced in the hot spots, but drop to normal low values just outside the hot spots.

A complete theory accounting for all of these results is beyond the scope of this paper. Instead, we present a simple, illustrative model which accounts for some of the essential features of the observations and reveals a further requirement of a more satisfactory model. We adopt the model which Hundhausen and Gentry (1968) have successfully used to simulate the formation and motion of driven shocks and blast waves in the solar wind. The mass, momentum, and energy equations governing the density, speed, pressure and internal energy density are given in Hundhausen and Gentry (1968). The system of equations is closed with the equation of state, $P = 2/3\ \rho I$, where the specific internal energy is $I = 3kT/(m_p+m_e)$. This is a single-fluid model for spherically symmetric flow. A high speed stream is generated by raising the source temperature (at .1 AU) as shown by the insert in Figure 9. This new stream advanced into a steady state flow for which $n=5\ cm^{-3}$, $V = 275$ km/sec and $T = 2 \times 10^{4}{}^{o}K$ at 1 AU. The resulting profiles of n, V, and T which would be seen by an observer at 1 AU are shown in Figure 9. This shows that a) $\Delta T \sim 5 \times 10^{4}{}^{o}K$, b) the temperature peaks at the inflection point in the V(t) curve, c) the density peaks ahead of the temperature, when V just begins to increase, and the maximum density is ~3 times the initial value. These results are consistent with results 1 to 6 above. The model fails to account for 8 because it is a single fluid model and neglects thermal conduction. It fails to account for 9 because it neglects $\underset{\sim}{B}$. Figure 9 shows velocity gradients occurring over a ~25 hour interval. A model which uses a jet rather than a spherically symmetric stream would give larger gradients.

We conclude that non-steady, non-linear, adiabatic compressional heating can account for the essential features of the proton density and temperature profiles, but a hydromagnetic 3-fluid model with heat conduction will be required accounting for the other observations.

Acknowledgements

The authors thank the principal investigator of the magnetic field experiment, Dr. N. F. Ness for his data. We are also indebted to Drs. Forslund, Hundhausen, Lashinsky, Tidman and Whang for fruitful discussions. The solar wind model of Hundhausen and Gentry was used to get the results in Figure 9.

The Vela 4B data was obtained as a part of the Vela Nuclear Test Detection Satellite Program which is jointly sponsored by the Advanced Research Project Agency of the Department of Defense and the U. S. Atomic Energy Commission and is managed by the U. S. Air Force.

REFERENCES

Barnes, A. 1966, Physics Fluids, 9, 1483.

Barnes, A. 1970, EOS Trans. Am. Geophys. Union, 51, 412.

Behannon, K. W., Fairfield, D. H. and Ness, N. F. 1968, NASA-GSFC Technical Report X-616-68-372.

Burlaga, L. F. and Ogilvie, K. W. 1968, J. Geophys. Res., 73, 6167.

Burlaga, L. F. and Ogilvie, K. W. 1970, Ap. J., 159, in press.

Davis, L., Smith, E. J., Coleman, P. J. and Sonett, C. P. 1966, in The Solar Wind", p. 35, ed. by R. J. Mackin, Jr., and Marcia Neugebauer, Pergamon Press.

Fairfield, D. H. 1969, J. Geophys. Res., 74, 3541.

Hundhausen, A. J., Asbridge, J. R. Bame, S. J., Gilbert, H. E., and Strong, I. B. 1967, J. Geophys. Res., 72, 87.

Hundhausen, A. J. and Gentry, R. A. 1969, J. Geophys. Res., 74, 2908.

Jokipii, J. R. and Davis, L., Jr. 1969, Ap. J. 156, 1101.

Lazarus, A. J., Bridge, H. S., and Davis, J. M. 1967, in Space Research VII, p.1296 , North-Holland Publishing Co. Amsterdam

Lazarus, A. J., Ogilvie, K. W. and Burlaga, L. F. 1970, submitted to Solar Physics.

Montgomery, M. D., Bame, S. J. and Hundhausen, A. J., 1968, J. Geophys. Res., 73, 4999.

Montgomery, M. D., Asbridge, J. R., and Bame, S. J. 1970, J. Geophys. Res., 75, 1217.

Neugebauer, Marcia and Snyder, C. W. 1966a, J. Geophys. Res., 71, 4469.

Neugebauer, Marcia, and Snyder, C. N. 1966b, in The Solar Wind, p. 21, Ed. by R. J. Mackin, Sr., and Marcia Neugebauer, Pergamon Press.

Neugebauer, Marcia, and Snyder, C. W. 1967, J. Geophys. Res., 72, 1823.

Ogilvie, K. W., Burlaga, L. F., and Wilkerson, T. W. 1968, J. Geophys. Res., 73, 6809.

Ogilvie, K. W. and Wilkerson, T. D. 1969, Solar Physics, 8, 435.

Ogilvie, K. W., McIlwraith, N., and Wilkerson, T. D. 1968, Rev. Sci. Inst., 39, 441.

Robbins, D. E., Hundhausen, A. J., and Bame, S. J. 1970, J. Geophys. Res., 75,1178.

Sari, J. W. and Ness, N. F. 1969, Solar Physics, 8, 155.

FIGURE CAPTIONS

Fig. 1 This shows plasma and magnetic field data in front of, within, and behind a hot spot. The continuous histograms are from Explorer 34 data, the broken histograms are from Vela 4B. See the text for the meaning of the symbols and the interpretation of these results.

Fig. 2 See Figure 1.

Fig. 3 See Figure 1.

Fig. 4 The histograms on top in each panel show 3-hr averages of ΔT for the events in Figures 1, 2, and 3. The histogram at the bottom, also based on 3-hr averages, shows the fractional change of bulk speed corresponding to each ΔT. This shows that the heating is largest at or somewhat behind the region where the deceleration is greatest.

Fig. 5 The panel on the left shows the typical power in the compressional mode in a hot spot (top histogram) and just outside it (bottom histogram). The right panel shows the corresponding powers in the transverse mode. The dashed lines show f^{-1} and f^{-2} spectra.

Fig. 6 This shows that power in the transverse modes is higher than in the longitudinal modes, and that it is high in the hot spot but not outside it.

Fig. 7 For a Maxwellian velocity distribution, $C_{calc} = C_{obs}$. This figure shows that to zeroth order this is true in both the hot spots (right panel) and in the regions just

outside the hot spots (left panel). Solid dots and open circles are points with $V_i < V$ and $V_i > V$, respectively. The separation between the dots and circles, due to the usual high energy tail of the distribution, is the same in the hot spots as outside them. Thus, to first order there is nothing unusual about the form of the proton spectra in hot spots.

Fig. 8 This shows that the α temperature in proportion to the proton temperature with the ratio being 4 even in the hot spot on day 181.

Fig. 9 The adiabatic solar wind model of Hundhausen and Gentry was used to generate the bulk speed gradient shown here. Note that the temperature peaks near the maximum gradient in V, while the density peaks ahead of it.

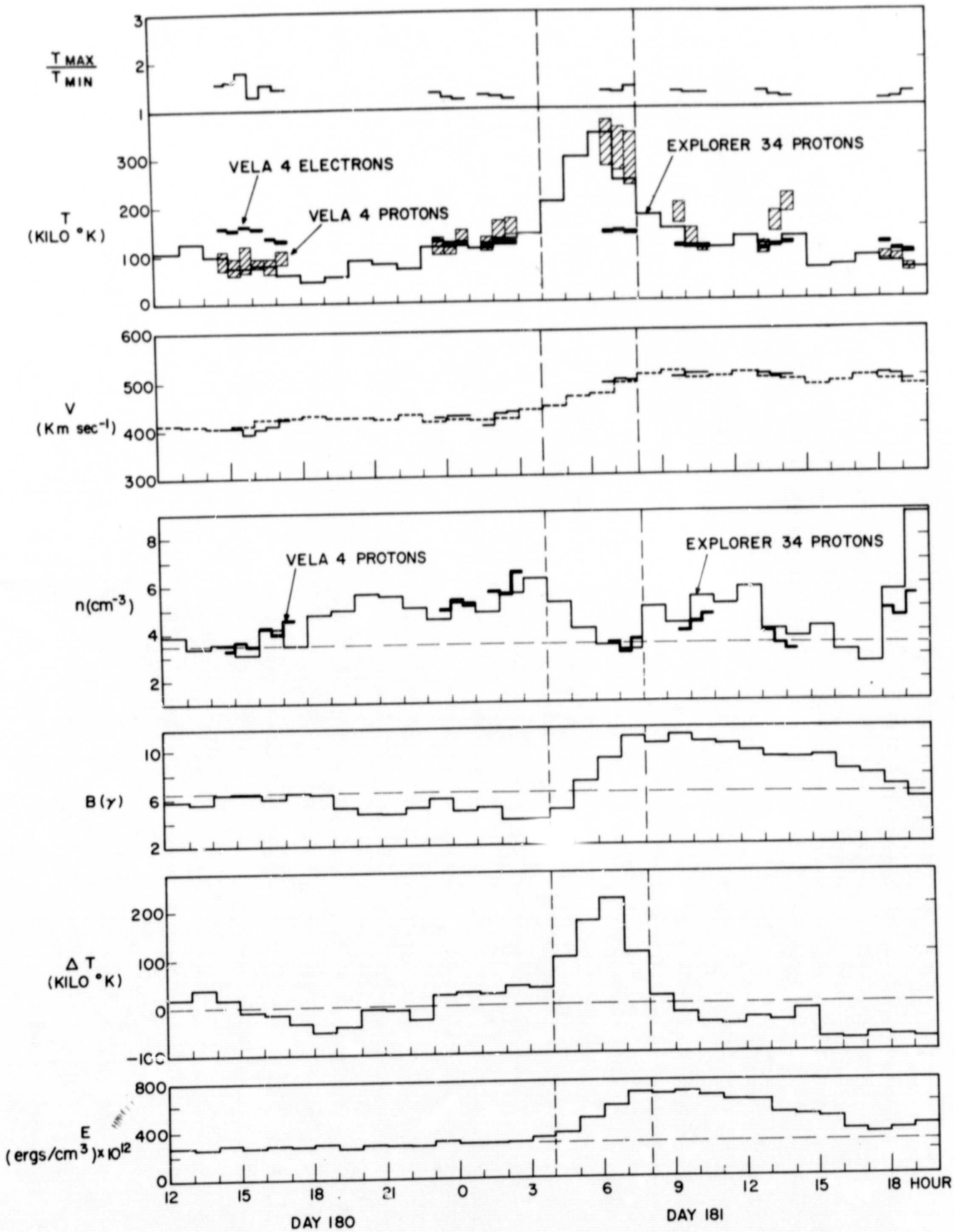
T MAX / T MIN
T (KILO °K)
VELA 4 ELECTRONS
VELA 4 PROTONS
EXPLORER 34 PROTONS
V (Km sec⁻¹)
n(cm⁻³)
VELA 4 PROTONS
EXPLORER 34 PROTONS
B(γ)
Δ T (KILO °K)
E (ergs/cm³)x10¹²
12 15 18 21 0 3 6 9 12 15 18 HOUR
DAY 180
DAY 181

Figure 1

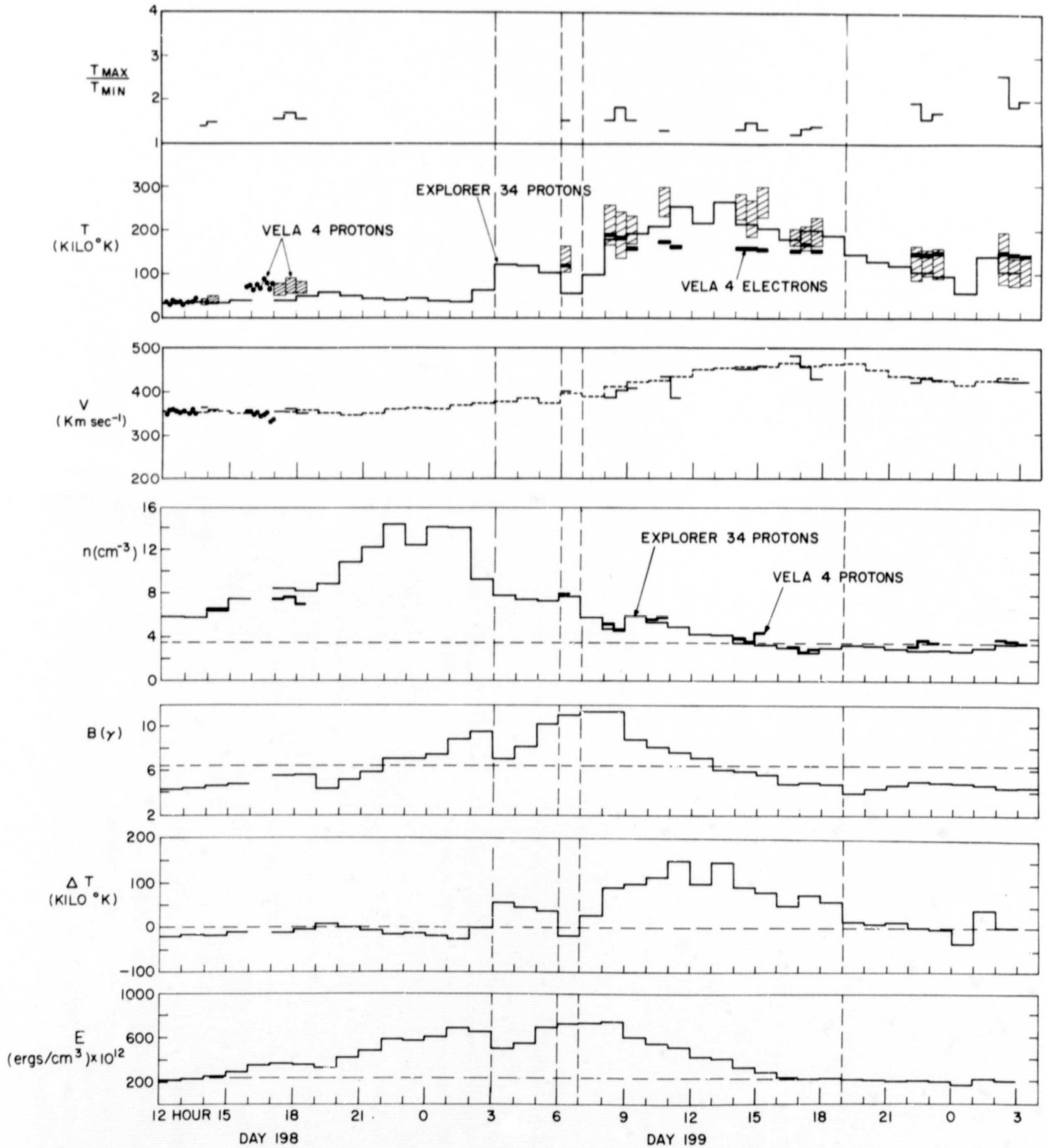
$\frac{T_{MAX}}{T_{MIN}}$
T (KILO °K)
EXPLORER 34 PROTONS
VELA 4 PROTONS
VELA 4 ELECTRONS
V (Km sec^{-1})
n(cm^{-3})
EXPLORER 34 PROTONS
VELA 4 PROTONS
B(γ)
Δ T (KILO °K)
E (ergs/cm^3)x10^{12}
12 HOUR 15 18 21 0 3 6 9 12 15 18 21 0 3
DAY 198
DAY 199

Figure 2

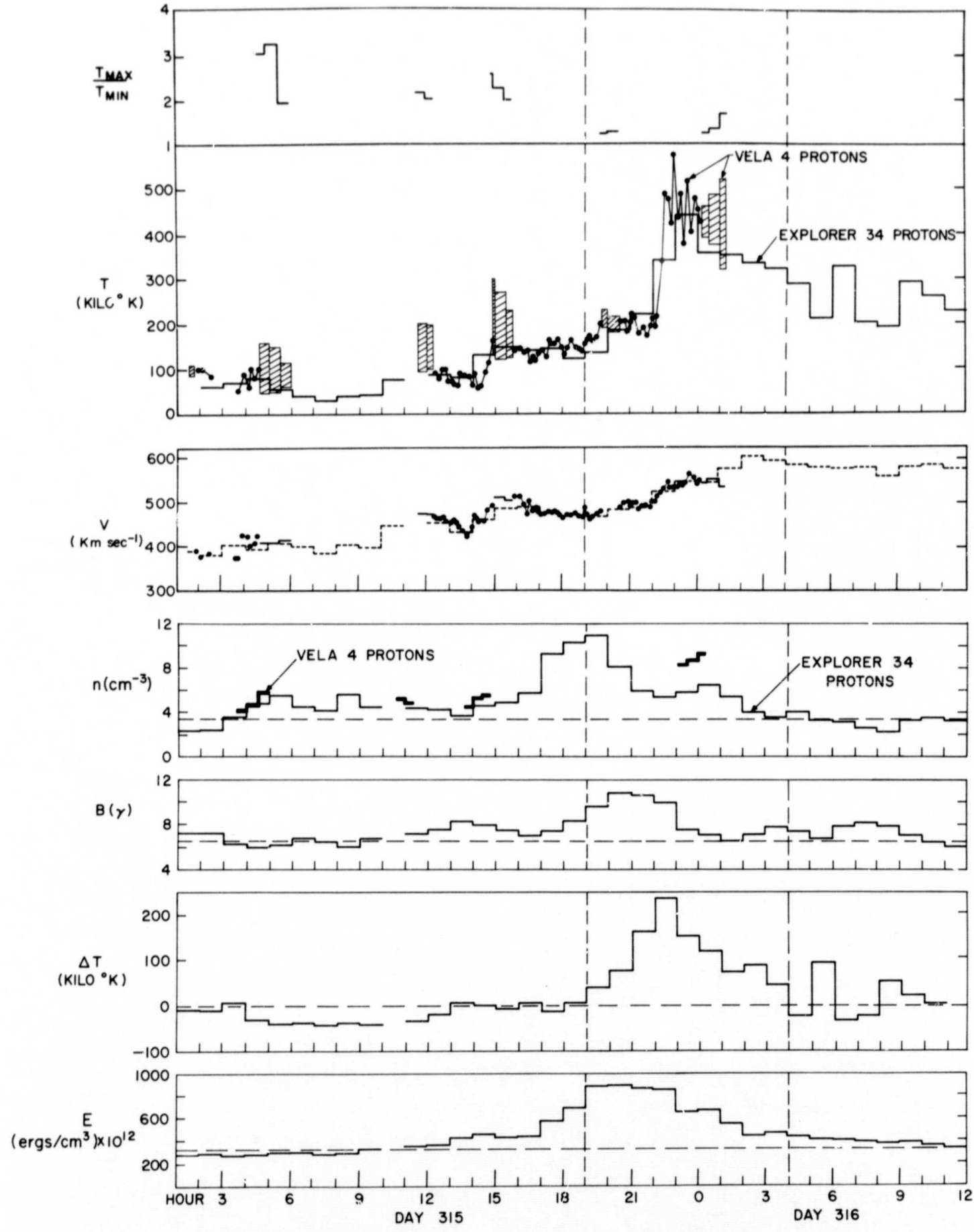
$\frac{T_{MAX}}{T_{MIN}}$
VELA 4 PROTONS
EXPLORER 34 PROTONS
T (KILO° K)
V (Km sec^{-1})
n(cm^{-3})
VELA 4 PROTONS
EXPLORER 34 PROTONS
B(γ)
ΔT (KILO °K)
E (ergs/cm^3)x10^{12}
HOUR 3 6 9 12 15 18 21 0 3 6 9 12
DAY 315
DAY 316

Figure 3

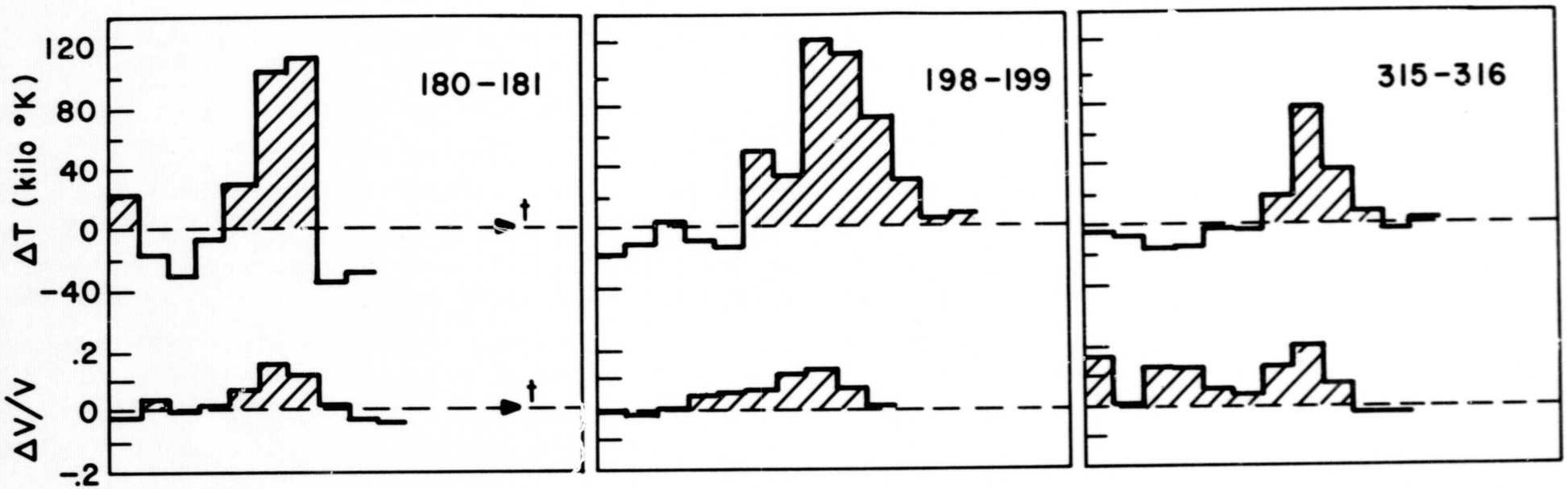

Figure 4

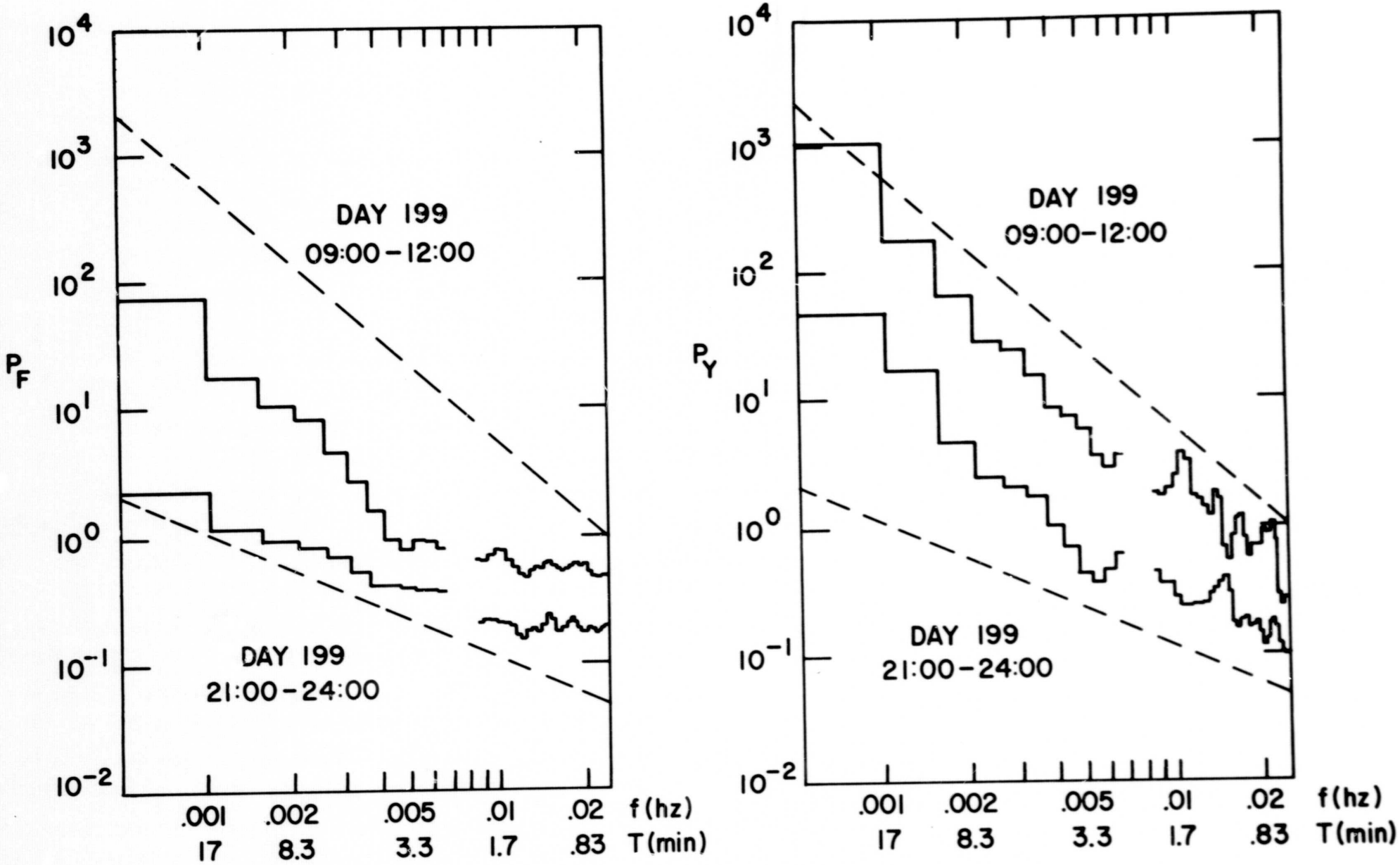
10^4
10^3
10^2
10^1
10^0
10^{-1}
10^{-2}
P_F
DAY 199
09:00-12:00
DAY 199
21:00-24:00
.001
.002
.005
.01
.02
f(hz)
17
8.3
3.3
1.7
.83
T(min)
P_Y
DAY 199
09:00-12:00
DAY 199
21:00-24:00

Figure 5

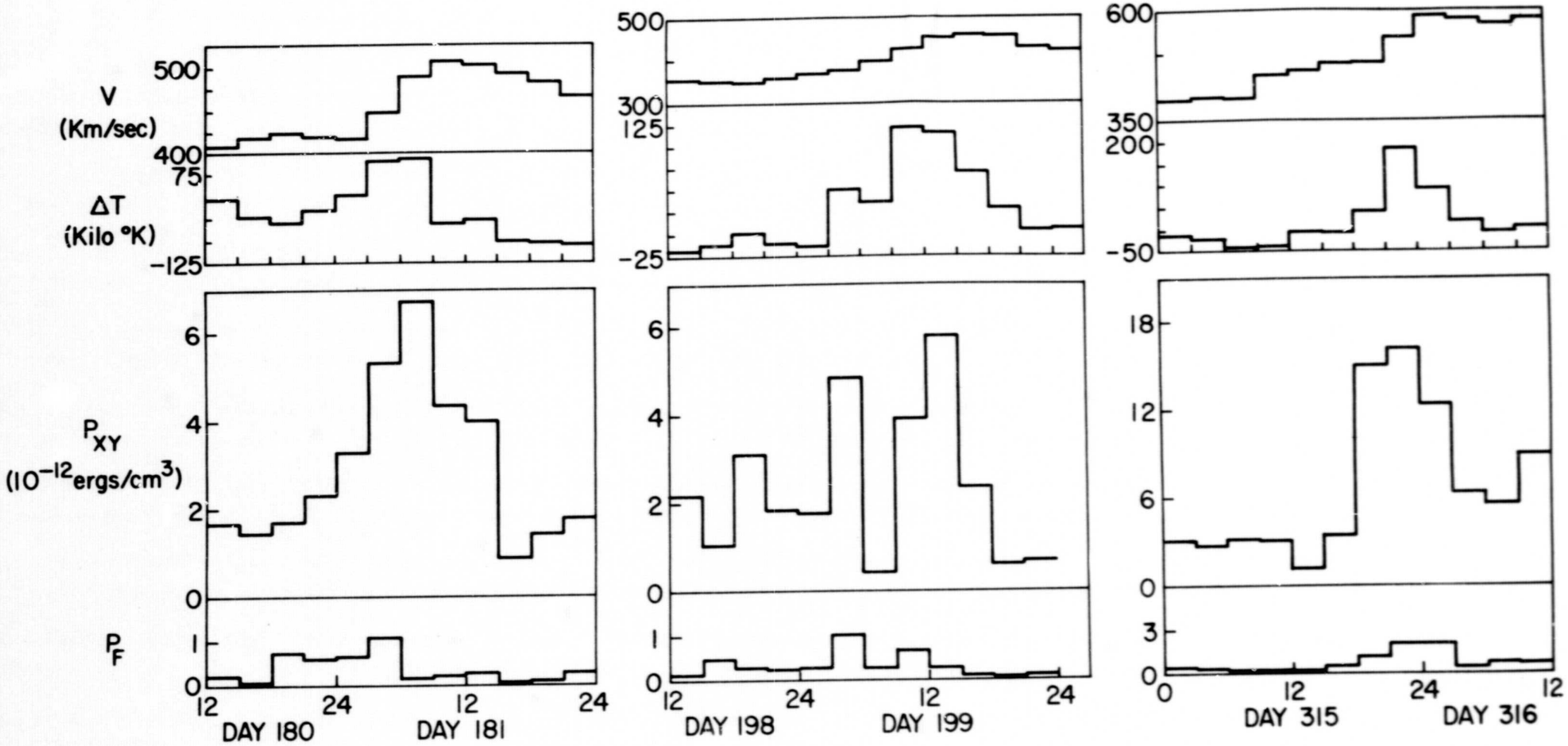
V
(Km/sec)
ΔT
(Kilo °K)
P_{XY}
(10^{-12}ergs/cm^3)
P_F
DAY 180
DAY 181
DAY 198
DAY 199
DAY 315
DAY 316

Figure 6

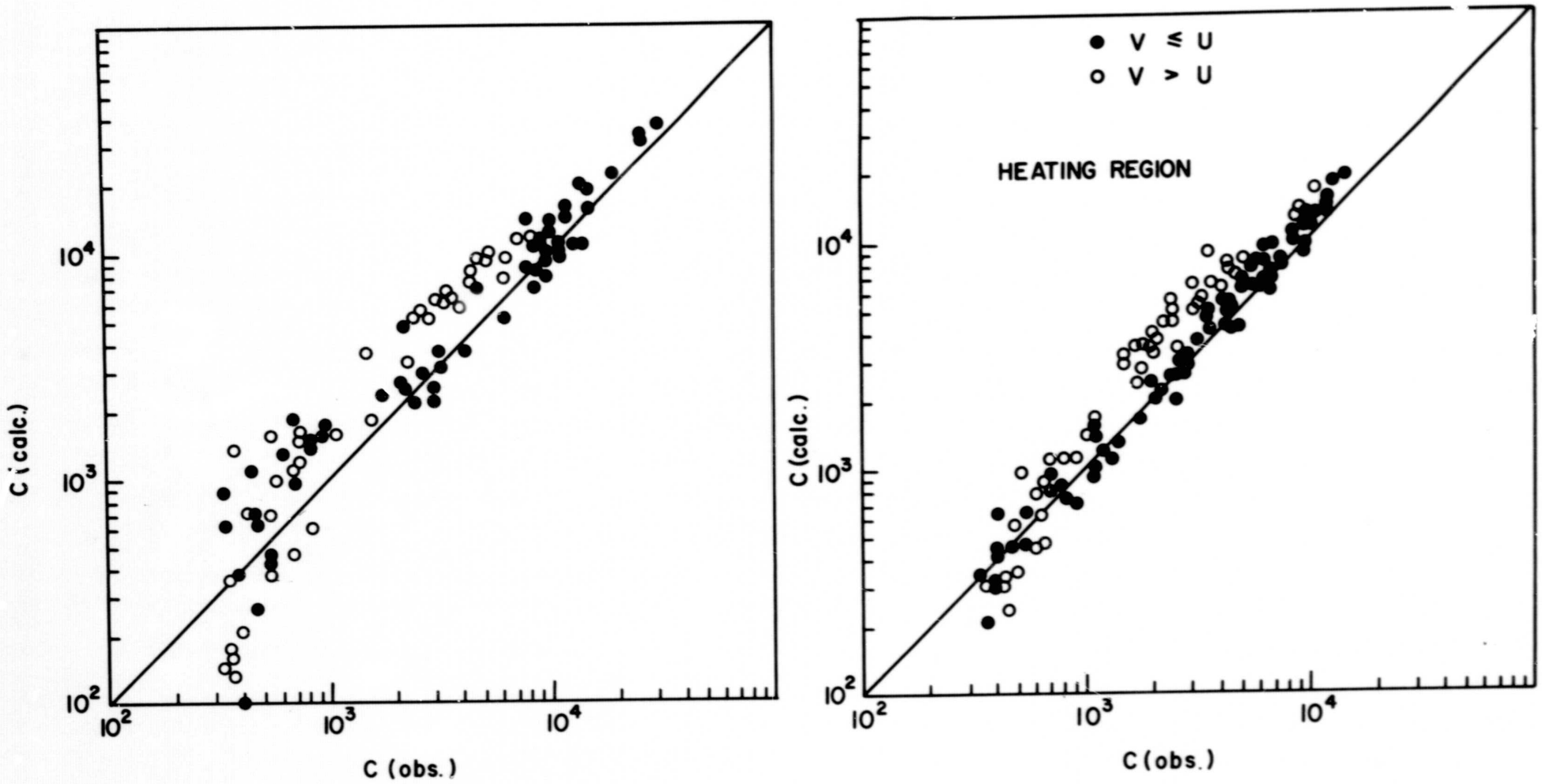

Figure 7

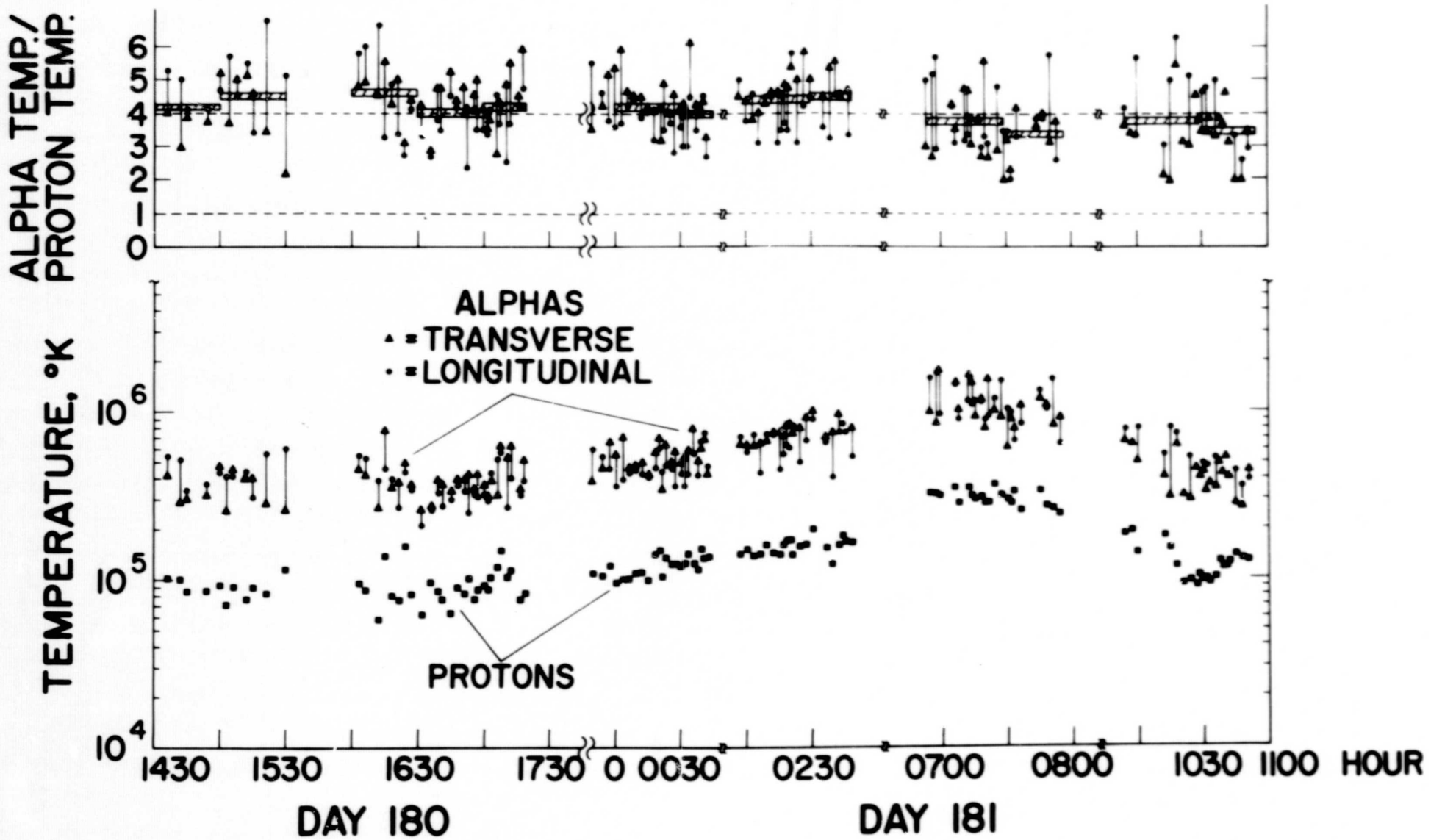
ALPHA TEMP./
PROTON TEMP.
0
1
2
3
4
5
6
TEMPERATURE, °K
10^6
10^5
10^4
ALPHAS
▲ = TRANSVERSE
• = LONGITUDINAL
PROTONS
1430
1530
1630
1730
0
0030
0230
0700
0800
1030
1100
HOUR
DAY 180
DAY 181

Figure 8

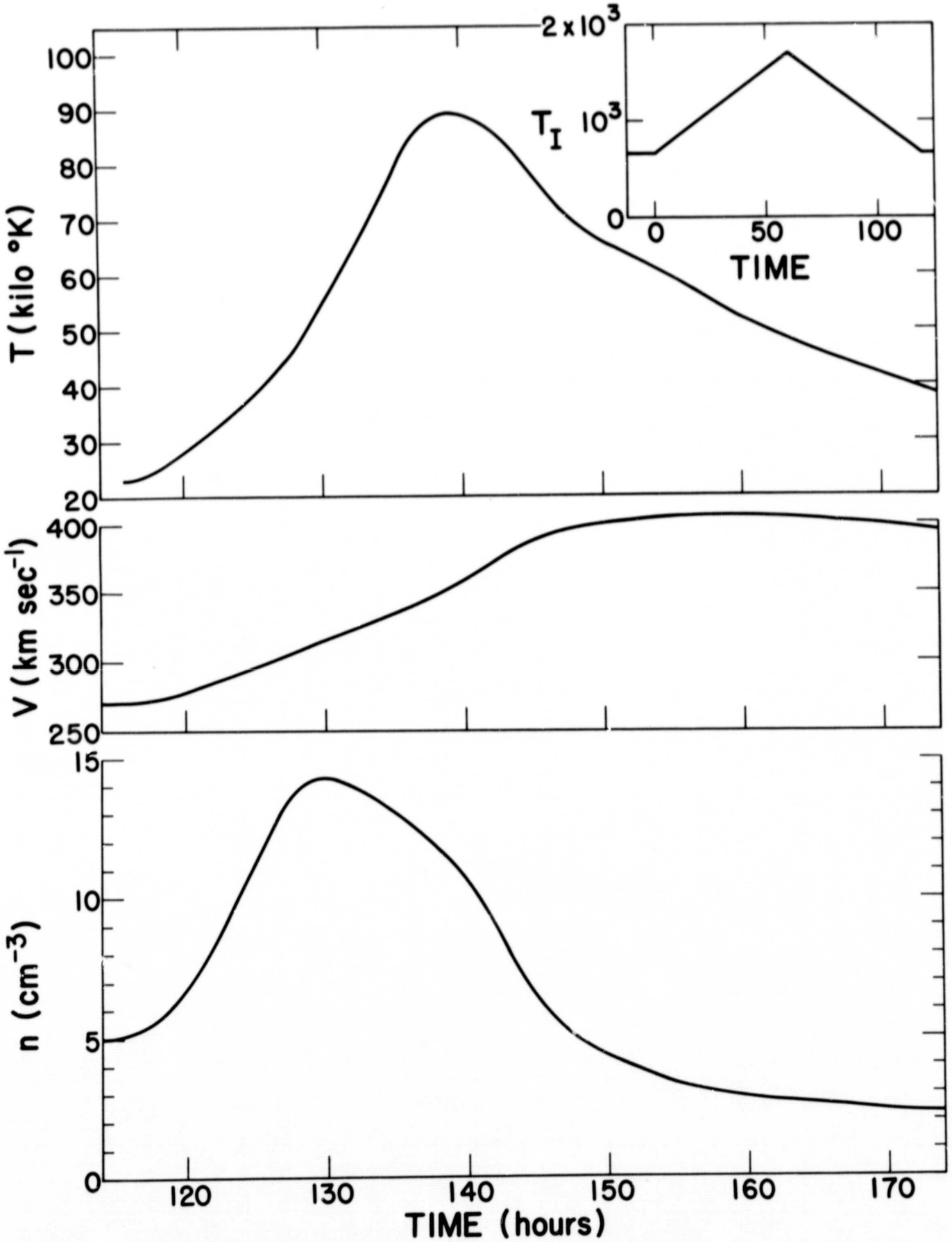
T (kilo °K)
100
90
80
70
60
50
40
30
20
2 x 10^3
T_I
10^3
0
0
50
100
TIME
V (km sec^-1)
400
350
300
250
n (cm^-3)
15
10
5
0
120
130
140
150
160
170
TIME (hours)

Figure 9